

# SEISMIC FRAGILITY ANALYSIS OF STRUCTURES WITH TUNED MASS DAMPERS BASED ON ENERGY BALANCE

Kevin K. F. Wong<sup>1</sup> and John L. Harris<sup>2</sup>

**ABSTRACT:** The ability of using tuned mass damper (TMD) to improve the structures' ability to dissipate earthquake input energy is investigated from the seismic fragility point of view. Nonlinear material behavior of the structure is modeled using the force analogy method, which is the backbone of analytically characterizing the plastic energy dissipation in the structure. Numerical analyses based on 100 simulated non-stationary Gaussian earthquake ground motions were performed to study the global responses and local energy dissipation of a six-story moment-resisting steel frame with and without TMD installed. The effectiveness of TMD based on the reduction of seismic responses and enhancement of the seismic fragility of the structure is considered at various structural performance levels, which include immediate occupancy, life safety, and collapse prevention. An "equivalent monotonic plastic strain" approach is used to correlate the seismic fragilities at different global performance levels with local damage in the structure. Results show that the use of TMD enhances the structures' ability to dissipate energy at low to moderate levels of the earthquake, but may be ineffective during a major earthquake that causes excessive damage in the structure.

*Keywords:* Structural Dynamics, Force Analogy Method, Energy Dissipation, Plastic Energy, Drift Ratio, Ductility, Plastic Strain

---

<sup>1</sup> Research Structural Engineer, National Institute of Standards and Technology, Email: kfwong@nist.gov

<sup>2</sup> Research Structural Engineer, National Institute of Standards and Technology, Email: jay.harris@nist.gov

## INTRODUCTION

A major problem in earthquake engineering that requires much research is the quantification of structural damage and its correlation with performance levels. The use of “damage parameters” or “damage functions” that relates seismic demands with structural capacities under cyclic loading is one way of representing structural “damage” in terms of mathematical terminology. The most common damage measure is inter-story drift ratio (Wang et al. 2007, Erduran and Yakut 2007, Yakut and Yilmaz 2008), which gives a good indication of the overall global response but lacks the specific detail and location of damage. Another common damage measure is ductility (Jarenprasert et al. 2006, Hong and Hong 2007), where damage is measured as a ratio of demand to capacity under a monotonic loading, but it lacks the ability to quantify cumulative damage when the structure is loaded cyclically. Other methods consider the effective distribution of plastic cycles and generalize the law of cumulative fatigue to the structural damage. However, some experiments have already demonstrated that high cycles of insignificant inelastic deformation are of no practical relevance to the degree of structural damage under major earthquake events (Cosenza et al. 1993).

To evaluate the structural performance and the damage level caused by an earthquake, a damage measure expressed in terms of energy seems most appropriate (Benavent-Climent 2007, Bojorquez et al. 2008). Because energy is derived from displacement and at the same time it has the ability to measure the cumulative effects, damage will become quantifiable when energy demand is compared with the corresponding energy capacity. More than two decades ago, McCabe and Hall (1989) have already introduced the energy spectra in addition to the ductility spectra and developed a damage index that depends on the energy dissipated under both positive

and negative hysteretic loops. However, the calculated energy was not based on any theoretical analysis but was simply computed based on ductility and equivalent cycles.

Two damage models that accounts for the maximum deformation and energy dissipation have been given great attention. In Bannon and Veneziano (1982), the damage index is set in a probabilistic context where the plastic energy is normalized with respect to the absorbed energy at the elastic limit. In Park and Ang (1985), the damage index is expressed as a linear combination of indices caused by excessive deformation and the effect of repeated cyclic loading. However, none of these studies has explicitly considered energies and their transfer induced by plastic deformation that actually causes damage to structures.

While it seems that structural damage can be quantified by accounting for the energy dissipation, no research has been found on quantifying structural damage based on plastic strain. Recognizing strain is already a dimensionless quantity that may be appropriate to serve as a damage measure, this research attempts to quantify structural damage by correlating the performance levels set forth in FEMA 440 (2005) with the local plastic energy dissipation and the corresponding equivalent plastic strain in a moment-resisting steel frame. Fragility analysis based on 100 simulated non-stationary Gaussian earthquake ground motions is used in the correlation, since fragility curves have been demonstrated to be a useful engineering tool in estimating the probability of reaching a certain structural performance level under a set of ground motions of a specified magnitude (Nielson and DesRoches 2007, Kafali and Grigoriu 2007, Zareian and Krawinkler 2007). Furthermore, recent studies have shown that the fragility curves for a certain structure can be noticeably altered simply by the implementation of structural retrofitting measures (Padgett and DesRoches 2008). Therefore, in this paper, tuned mass damper (TMD) is applied to improve structural performance and reduce structural damage.

## FORCE ANALOGY METHOD

The force analogy method is tool of conducting nonlinear analysis of structures, either static or dynamic, based on a change in displacement field instead of stiffness to give the total force in the structure. The overall procedure has been discussed in Wong and Yang (1999). Because of its importance in analytically quantifying the plastic energy in the energy balance equation, this method is briefly summarized here.

Consider structure modeled as an  $n$ -degree of freedom (DOF) system, the displacement can be written in a vector form as

$$\mathbf{x}(t) = \mathbf{x}'(t) + \mathbf{x}''(t) = \begin{Bmatrix} x'_1(t) \\ x'_2(t) \\ \vdots \\ x'_n(t) \end{Bmatrix} + \begin{Bmatrix} x''_1(t) \\ x''_2(t) \\ \vdots \\ x''_n(t) \end{Bmatrix} \quad (1)$$

where  $\mathbf{x}(t)$  represents the total displacement vector,  $\mathbf{x}'(t)$  is the elastic displacement vector that returns to zero after the earthquake has subsided, and  $\mathbf{x}''(t)$  is the inelastic displacement vector that represents the permanent deformation of the structure (see Figure 1).

Similar to displacements, the total moments  $\mathbf{m}(t)$  and plastic rotations  $\Theta''(t)$  at the plastic hinge locations (PHLs) on the structure in the moment-resisting frame can also be represented in vector forms as

$$\mathbf{m}(t) = \mathbf{m}'(t) + \mathbf{m}''(t) = \begin{Bmatrix} m'_1(t) \\ m'_2(t) \\ \vdots \\ m'_m(t) \end{Bmatrix} + \begin{Bmatrix} m''_1(t) \\ m''_2(t) \\ \vdots \\ m''_m(t) \end{Bmatrix}, \quad \Theta''(t) = \begin{Bmatrix} \theta''_1(t) \\ \theta''_2(t) \\ \vdots \\ \theta''_m(t) \end{Bmatrix} \quad (2)$$

where  $\mathbf{m}'(t)$  is the elastic moment vector due to elastic displacement and  $\mathbf{m}''(t)$  is the inelastic moment vector due to inelastic displacement. The value  $m$  represents the total number of PHLs

identified in the structure. The inelastic moment  $\mathbf{m}''(t)$  and inelastic displacement  $\mathbf{x}''(t)$  exist when plastic rotations  $\Theta''(t)$  occur at certain PHLs in the structure. The relationships after imposing equilibrium and compatibility conditions are given by the formula:

$$\mathbf{m}''(t) = -(\mathbf{K}'' - \mathbf{K}'^T \mathbf{K}^{-1} \mathbf{K}') \Theta''(t) \quad (3)$$

$$\mathbf{x}''(t) = \mathbf{K}^{-1} \mathbf{K}' \Theta''(t) \quad (4)$$

where  $\mathbf{K}'$  is the  $n \times m$  stiffness matrix that relates the plastic rotation  $\Theta''(t)$  with the restoring forces at the global DOFs,  $\mathbf{K}$  is the  $n \times n$  global stiffness matrix, and  $\mathbf{K}''$  is the  $m \times m$  stiffness matrix that relates the plastic rotation  $\Theta''(t)$  with the restoring moments at the PHLs.

The elastic moment  $\mathbf{m}'(t)$  at each PHL relates directly to the elastic displacement  $\mathbf{x}'(t)$  of the structure, which in turn is caused by applying the force  $\mathbf{f}_s(t)$  on the global structure. The relationship can be written as:

$$\mathbf{f}_s(t) = \mathbf{K} \mathbf{x}'(t) \quad (5)$$

$$\mathbf{m}'(t) = \mathbf{K}'^T \mathbf{x}'(t) \quad (6)$$

Substituting Eqs. (4) and (5) into Eq. (1) gives

$$\mathbf{x}(t) = \mathbf{K}^{-1} \mathbf{f}_s(t) + \mathbf{K}^{-1} \mathbf{K}' \Theta''(t) \quad (7)$$

Since the elastic displacement  $\mathbf{x}'(t)$  is defined in the way as shown in Figure 1, Eq. (7) shows that the total displacement  $\mathbf{x}(t)$  in the structure contains two distinctive parts, one due to the applied force and the other due to the material nonlinearity of the structure. This distinction facilitates the separation of strain energy and plastic energy to be discussed in the next section.

Performing matrix manipulations on Eqs. (1) through (6) gives the governing equation of the force analogy method, which is

$$\mathbf{m}(t) + \mathbf{K}'' \Theta''(t) = \mathbf{K}'^T \mathbf{x}(t) \quad (8)$$

Equations (4) and (8) represent the essence of the force analogy method, as they are used in each and every time steps in the dynamic analysis to calculate the nonlinear structural responses.

## ENERGY BALANCE EQUATION

During an earthquake, input energy ( $IE$ ) caused by ground motion enters the structure and converts into different energy forms in the structure, and these energy forms include the strain energy ( $SE$ ), kinetic energy ( $KE$ ), damping energy ( $DE$ ), and plastic energy ( $PE$ ). According to Uang and Bertero (1990), using absolute energy to characterize the seismic energy in structures is more reasonable than using relative energy because kinetic energy should be expressed in terms of absolute velocity of the structure. Therefore, in this research, the energy balance equation is based on the absolute energy method. Consider the equation of motion with the global stiffness force given in Eq. (5):

$$\mathbf{M}\ddot{\mathbf{x}}(t) + \mathbf{C}\dot{\mathbf{x}}(t) + \mathbf{f}_s(t) = -\mathbf{M}\ddot{\mathbf{g}}(t) \quad (9)$$

where  $\mathbf{M}$  is the  $n \times n$  non-zero mass matrix,  $\mathbf{C}$  is the  $n \times n$  damping matrix,  $\ddot{\mathbf{g}}(t)$  is the  $n \times 1$  earthquake ground acceleration corresponding to each DOF, and a dot above the variable represents the derivative of the variable with respect to time.

Define the absolute displacement  $\mathbf{y}(t)$  of an  $n$ -DOF structure to be the sum of relative displacement  $\mathbf{x}(t)$  and ground displacement  $\mathbf{g}(t)$ , then the equations for displacement, velocity, and acceleration can be written as:

$$\mathbf{y}(t) = \mathbf{x}(t) + \mathbf{g}(t) \quad , \quad \dot{\mathbf{y}}(t) = \dot{\mathbf{x}}(t) + \dot{\mathbf{g}}(t) \quad , \quad \ddot{\mathbf{y}}(t) = \ddot{\mathbf{x}}(t) + \ddot{\mathbf{g}}(t) \quad (10)$$

Substituting Eq. (5) and the acceleration equation of Eq. (10) into Eq. (9) gives

$$\mathbf{M}\ddot{\mathbf{y}}(t) + \mathbf{C}\dot{\mathbf{x}}(t) + \mathbf{K}\mathbf{x}'(t) = \mathbf{0} \quad (11)$$

Integrating both sides of Eq. (11) over the path of structural response  $\mathbf{x}(t)$  from time 0 to time  $t_k$  gives

$$\int_{t=0}^{t=t_k} \ddot{\mathbf{y}}^T \mathbf{M} d\mathbf{x} + \int_{t=0}^{t=t_k} \dot{\mathbf{x}}^T \mathbf{C} d\mathbf{x} + \int_{t=0}^{t=t_k} \mathbf{x}'^T \mathbf{K} d\mathbf{x} = 0 \quad (12)$$

Since  $d\mathbf{x}(t) = d\mathbf{y}(t) - d\mathbf{g}(t)$  based on displacement equation of Eq. (10), substituting this equation into the first term of Eq. (12) gives

$$\int_{t=0}^{t=t_k} \ddot{\mathbf{y}}^T \mathbf{M} d\mathbf{y} + \int_{t=0}^{t=t_k} \dot{\mathbf{x}}^T \mathbf{C} d\mathbf{x} + \int_{t=0}^{t=t_k} \mathbf{x}'^T \mathbf{K} d\mathbf{x} = \int_{t=0}^{t=t_k} \ddot{\mathbf{y}}^T \mathbf{M} d\mathbf{g} \quad (13)$$

The first and second terms of Eq. (13) represent  $KE$  and  $DE$ , respectively, and the term on the right side of Eq. (13) represents  $IE$ .

The third term on the left side of Eq. (13) relates to the energy due to stiffness, which contains both linear (i.e.,  $SE$ ) and nonlinear (i.e.,  $PE$ ) components. By taking advantage of Eq. (1), these two energy components can be separated very simply as shown in Figure 1. Representing Eq. (1) in incremental form,  $d\mathbf{x}(t) = d\mathbf{x}'(t) + d\mathbf{x}''(t)$ , and substituting this result into the third term of Eq. (13) gives

$$\int_{t=0}^{t=t_k} \mathbf{x}'^T \mathbf{K} d\mathbf{x} = \int_{t=0}^{t=t_k} \mathbf{x}'^T \mathbf{K} d\mathbf{x}' + \int_{t=0}^{t=t_k} \mathbf{x}'^T \mathbf{K} d\mathbf{x}'' \quad (14)$$

It is observed that the first term on the right side of Eq. (14) gives the strain energy, i.e.,

$$SE = \int_{t=0}^{t=t_k} \mathbf{x}'^T \mathbf{K} d\mathbf{x}' = \frac{1}{2} \mathbf{x}'^T(t_k) \mathbf{K} \mathbf{x}'(t_k) \quad (15)$$

Now consider the last term of Eq. (14) based on the force analogy method. Rewriting Eq. (4) as  $d\mathbf{x}'' = \mathbf{K}^{-1} \mathbf{K}' d\Theta''$  and Eq. (6) as  $\mathbf{m}'^T = \mathbf{x}'^T \mathbf{K}'$ , and substituting these results into the last term of Eq. (14) gives

$$\int_{t=0}^{t=t_k} \mathbf{x}'^T \mathbf{K} d\mathbf{x}'' = \int_{t=0}^{t=t_k} \mathbf{x}'^T (\mathbf{K} \mathbf{K}^{-1}) \mathbf{K}' d\Theta'' = \int_{t=0}^{t=t_k} \mathbf{x}'^T \mathbf{K}' d\Theta'' = \int_{t=0}^{t=t_k} \mathbf{m}'^T d\Theta'' \quad (16)$$

This term represents the total  $PE$  dissipated in the structure, and it accounts for the contribution of all plastic hinges. Since Eq. (16) is calculated by multiplying the elastic moment vector  $\mathbf{m}'(t)$  with the change in plastic rotation vector  $d\Theta''(t)$ , this equation can therefore be represented by the sum of plastic energy dissipated at each plastic hinge, i.e.,

$$PE = \int_{t=0}^{t=t_k} \mathbf{m}'^T d\Theta'' = \int_{t=0}^{t=t_k} \sum_{i=1}^m m'_i d\theta''_i = \sum_{i=1}^m \int_{t=0}^{t=t_k} m'_i d\theta''_i = \sum_{i=1}^m PE_i \quad (17)$$

where  $PE_i$  represents the plastic energy dissipated at the  $i$ th plastic hinge:

$$PE_i = \int_{t=0}^{t=t_k} m'_i d\theta''_i \quad (18)$$

Therefore, in summary, Eq. (13) can be written in terms of energy balance as

$$KE + DE + SE + PE = IE \quad (19)$$

## STRUCTURAL MODEL WITH TUNED MASS DAMPER

The use of TMD, a passive control device, in structures has been demonstrated to be effective in reducing the dynamic response due to lateral loadings since the 1970's (McNamara 1977, Luft 1979). Since then, significant number of studies has been conducted to enhance the effectiveness of the TMDs, which include the use of multiple TMDs (Xu and Igusa 1992, Chen and Wu 2001, Johnson et al. 2003, Guo and Chen 2007, Qin et al. 2007), and active/semi-active TMDs (Li and Liu 2002, Nagarajaiah and Sonmez 2006, Li and Zhu 2007). Some design procedures have also been proposed (Abe and Fujino 1994, Hoang et al. 2008, Ueng 2008). However, most of these works mainly consider structures responding in the elastic domain, while research work related to structures with TMD responding in the inelastic domain is very limited.

Recognizing this drawback on the previous research, this study attempts to apply the force analogy method to conduct seismic fragility analysis of structures with TMDs responding

in the inelastic domain. A six-story moment-resisting steel frame shown in Figure 2 was used in the present study. It contains 6 DOFs with 40 PHLs. Let the mass of each floor be 300,000 kg and the damping be 3% in all six modes of the elastic structure. Based on the member sizes shown in Figure 2, the natural periods of vibration of all six elastic modes were calculated and summarized in Table 1. The plastic rotations were assumed to be concentrated at one point at the end of the beam and at the bottom of the columns. The moment capacity  $m_p$  was assumed to be equal to the plastic moment of the member, i.e.,

$$m_p = f_y Z \quad (24)$$

where  $f_y$  is the yield stress of steel of 248.2 MPa, and  $Z$  is the plastic section modulus of the member. All beams were subjected to a 21.89 kN/m uniform gravity loads prior to the beginning of the earthquake motion. Moment versus plastic rotation relationship of all plastic hinges was assumed to exhibit elastic-plastic behavior, and the effect of interaction between moment and axial force on the moment capacities of column members was neglected.

Tuned mass damper was installed at the roof level of the frame as shown in Figure 2. Let the mass be 10% of the total mass of the structure, which is  $m_{TMD} = 180,000$  kg. Noting that the fundamental period of vibration of the frame is 1.22 s as shown in Table 1, the TMD with a period  $T_{TMD} = 2.0$  s was selected. This resulted in a TMD stiffness of  $k_{TMD} = 565.5$  kN/m, and it was assumed to remain elastic during the seismic event. A critical damping ratio of  $\zeta_{TMD} = 5\%$  damping was assumed for the TMD, which gave a damping value of  $c_{TMD} = 56.5$  kN-s/m. Based on this setup, it follows that the  $7 \times 7$  damping and stiffness matrices of the frame with TMD installed are of the form:

$$\mathbf{C} = \begin{bmatrix} c_{11} & c_{12} & \cdots & c_{16} & 0 \\ c_{21} & c_{22} & \ddots & \vdots & \vdots \\ \vdots & \ddots & \ddots & c_{56} & 0 \\ c_{61} & \cdots & c_{65} & c_{66} + c_{TMD} & -c_{TMD} \\ 0 & \cdots & 0 & -c_{TMD} & c_{TMD} \end{bmatrix}, \quad \mathbf{K} = \begin{bmatrix} k_{11} & k_{12} & \cdots & k_{16} & 0 \\ k_{21} & k_{22} & \ddots & \vdots & \vdots \\ \vdots & \ddots & \ddots & k_{56} & 0 \\ k_{61} & \cdots & k_{65} & k_{66} + k_{TMD} & -k_{TMD} \\ 0 & \cdots & 0 & -k_{TMD} & k_{TMD} \end{bmatrix} \quad (25)$$

## EARTHQUAKE RECORDS

A suite of earthquake ground motions is always necessary in order to conduct research on seismic fragility analysis. In this study, one horizontal component of the ground acceleration  $\ddot{g}(t)$  was considered for the 2-dimensional frame, and it was modeled as a non-stationary Gaussian process with zero mean. It was constructed by multiplying a stationary random process  $S(t)$  by a deterministic temporal modulation function  $\phi(t)$  (Simulescu et al. 1989):

$$g(t) = \phi(t) \times S(t) \quad (26)$$

The formulation of Yeh and Wen (1990) for  $\phi(t)$  was used:

$$\phi(t) = \sqrt{A \frac{t^B}{D + t^E} e^{-Ct}} / \phi(t_0) \quad (27)$$

where  $A$ ,  $B$ ,  $C$ ,  $D$ , and  $E$  are constants, and  $\phi(t_0)$  is the normalizing factor set equal to maximum value of  $\phi(t)$  that occurs at  $t = t_0$ . The Clough-Penzien spectrum (Clough and Penzien 1975) was assumed for  $S(t)$ , which has zero mean and a two-sided power spectral density function of the form:

$$\Phi_{ss}(\omega) = \frac{\omega_g^4 + (2\zeta_g \omega_g \omega)^2}{(\omega_g^2 - \omega^2)^2 + (2\zeta_g \omega_g \omega)^2} \times \frac{\omega^2}{(\omega_f^2 - \omega^2)^2 + (2\zeta_f \omega_f \omega)^2} \times \Phi_0 \quad (28)$$

where  $\Phi_0$  represents the spectrum level (normalized to unit mass) of the broad-band excitation at the base,  $\omega_g$  and  $\zeta_g$  represents the characteristic frequency and damping ratio of the ground,

respectively, and  $\omega_f$  and  $\zeta_f$  represents the characteristic frequency and damping ratio of sub-filter, respectively.

A total of 100 earthquake ground acceleration time histories was generated based on the above procedure and then normalized to a peak ground acceleration (PGA) of 1.0g. Nonlinear dynamic analyses were performed using the 6-story moment-resisting steel frame shown in Figure 2 with and without TMD installed, and a typical time history response comparison is shown in Figure 3. As shown in this figure, there is typically no improvement in terms of displacement, velocity, and acceleration responses for using TMD when the structure is responding in the nonlinear domain, but there is a considerable improvement in increasing the damping energy dissipation while reducing the plastic energy dissipation when TMD is used. This shows, from the energy perspective, that TMD does in fact have the advantage of protecting the structure by reducing the damage caused by earthquakes.

Figure 4 shows the comparison of the average maximum responses of the 6-story frame due to all 100 simulated earthquake ground motions. Similar to the observation made for a single ground motion, there seems to be only slight reduction in the average maximum displacement and velocity responses when TMD is used, while there is practically no difference in the average maximum absolute acceleration, proving again that there is no enhancement of the nonlinear structural performance from the kinematic perspective when TMD is used. Figure 5 shows the comparison of average maximum energy responses due to all 100 simulated ground motions, both globally at the structure level and locally at the plastic hinge level. Again, similar to the observation made for the response due to a single ground motion, the TMD has the ability to protect the structure by reducing the plastic energy dissipation, both globally and locally. In

particular when TMD is used, a 25% reduction in local plastic energy dissipation is observed at PHLs #2 and #3, which are located at the base of the interior columns.

## SEISMIC FRAGILITY ANALYSIS

Incremental dynamic analyses of each earthquake ground motion record were performed on the 6-story moment-resisting steel frame with and without TMD installed by scaling the entire earthquake with a scaling factor. Because the original earthquake ground motion was normalized to a PGA of 1.0g, the scaling factor thus represents the resulting PGA of each earthquake. The number of exceedance of the performance levels was then counted. These performance levels include immediate occupancy (IO), life safety (LS), and collapse prevention (CP), and these limits for each performance level based on the maximum inter-story drift ratio set forth in the FEMA 440 document (FEMA 2005) is summarized in Table 2. Once the number of exceedance is determined, the data were then fitted using a log-normal distribution by the least square method to obtain the fragility function.

For this numerical study, in addition to using a tuned mass of 10% of the total structural mass to study the effect of TMD on the seismic fragility of structures, a further selection of TMD 20% of the total structural mass is also included. For a TMD of 20% mass, both the period of vibration and damping ratio were set to be the same as that of 10%, i.e.,  $T_{TMD} = 2.0$  s and  $\zeta_{TMD} = 5\%$ , and therefore the values of  $m_{TMD}$ ,  $c_{TMD}$ , and  $k_{TMD}$  are simply doubled. Figure 6 shows the comparison of fragilities of the structure with and without TMD installed. Several phenomena were observed:

- There is practically no difference in results between the choice of TMD with 10% mass and TMD with 20% mass in terms of seismic fragility of the structure.

- The use of TMD enhances the fragility of the structure at IO and LS performance levels (i.e., low to moderate earthquakes, or zero to moderate nonlinearity in the structure) by shifting the fragility curves to the right.
- TMD is ineffective at CP performance level (i.e., major earthquake, or large nonlinearity in the structure) in protecting the structure from collapse.

### **CORRELATION OF DAMAGE WITH PERFORMANCE LEVELS**

The performance levels used in this study and presented in Figure 6 were evaluated based on the drift ratio limits of the global structure, which is highly dependent the types of materials and properties used in the lateral resisting system of the structure. For example, if the structure is well designed and constructed, the structure can respond seismically to a higher level of displacement without suffering damage, and therefore the IO performance level has been achieved even at a larger drift ratio. In view of this, a more accurate way of measuring performance levels may come from the local damage associated with each level of earthquake ground motion. Therefore, an attempt to correlate damage with performance levels is investigated here by using fragility functions of the structure based on plastic energy dissipation and equivalent strain.

Similar to normalizing the inter-story drift response by dividing the value with respect to the corresponding story height to attain the maximum drift ratio, a normalization method for the plastic energy is here proposed as follow:

$$PE \text{ Ratio} = \max_i \left\{ \frac{PE_i}{f_y \times A_i \times d_i} \right\} \quad (29)$$

where  $A_i$  and  $d_i$  are respectively the cross-sectional area and depth of the corresponding member. While the plastic hinge length is assumed to be equal to  $d_i$ , the product of  $A_i$  and  $d_i$  therefore gives the volume of the plastic hinge. Finally, multiplying this plastic hinge volume with the yield stress of steel  $f_y$  gives an equivalent energy capacity of the member, which is the *PE Ratio* in Eq. (29) that can be used to benchmark across the different sizes of the member in the structure.

Another way of interpreting Eq. (29) is that when plastic energy  $PE_i$  is divided by the volume of the plastic hinge, i.e.,  $A_i \times d_i$ , plastic energy density is obtained. Since plastic energy density represents the area under the stress-strain curve of any material, further dividing this plastic energy density by the yield stress of steel  $f_y$  gives the equivalent plastic strain. Therefore, *PE Ratio* can be view as the maximum of the “equivalent monotonic plastic strain” experienced among all the plastic hinges, where strain hardening is not considered.

By selecting different *PE Ratio* limits, fragility curves were constructed and compared to the fragility curves based on drift ratios limits. The best correlation of *PE Ratio* limit and drift ratio limit were found, and the results are presented in Table 2 for each performance level. The mentality of correlating *PE Ratio* limit equal to zero with the IO performance level seems correct, since no structural damage should be expected in order to achieve immediate occupancy after an earthquake. For a yield strain of steel of 0.00125, a *PE Ratio* = 0.002 at the LS performance level corresponds to an “equivalent monotonic strain ductility”,  $\mu_{LS}$ , of

$$\mu_{LS} = \frac{0.00125 + 0.002}{0.00125} = 2.6 \quad (30)$$

Similarly, a *PE Ratio* = 0.02 at the CP performance level corresponds to an “equivalent monotonic strain ductility”,  $\mu_{CP}$ , of

$$\mu_{CP} = \frac{0.00125 + 0.02}{0.00125} = 17.0 \quad (31)$$

Figure 7 summarizes the correlation between *PE* Ratio limits and drift ratio limits at all three performance levels for the frame without TMD installed. Similarly, Figure 8 shows the same for the frame with TMD of 10% mass, and Figure 9 shows that with TMD of 20% mass. While there is a consistency in the correlation at both the LS and CP performance levels, these figures show that the drift ratio limit of 0.005 at the IO performance level is far below the threshold to yielding, indicating that conservatism has been built into the limit set forth in FEMA 440 (2005) at the IO performance level.

Similarly, note that a plastic strain of 0.02 represents a level where the steel material begins its strain hardening behavior. This means that equivalent monotonic plastic strain, or the *PE* Ratio, of 0.02 as the limit of the CP performance level is truly far away from fracture of the structural member, which indicates yet another level of conservatism has been built into the drift ratio limit set forth in FEMA 440 (2005) at the CP performance level.

Figure 10 compares the average of the 100 values for the *PE* Ratios of individual plastic hinge in the structure with and without TMD installed at a PGA of 0.8g, which corresponds to a level of earthquake ground motion that produces a 50% of exceedance of the LS performance level when TMD of 10% mass is used (see Figure 8). Similarly, Figure 11 compares the average *PE* Ratios of each plastic hinge in the structure with and without TMD installed at a PGA of 1.3g, which corresponds to a level of earthquake ground motion that produces a 50% of exceedance of the CP performance level when TMD of 10% mass is used. While the *PE* ratios are considerably lower when TMD is used (see Figure 10(b)) than without TMD (see Figure 10(a)) at the LS performance level, the difference is less evident in Figure 11 at the CP

performance level, which again proves that TMD is ineffective in protecting structures during a major earthquake.

A point worth mentioning in Figures 10 and 11 is that while TMD is effective in reducing the damage at the lower stories, it draws energy up to the structure to where the TMD is located. Therefore, larger *PE* ratios and damage are observed at the roof level, which is consistent with the conclusion obtained in Wong and Johnson (2009).

## CONCLUSION

In this research, the effectiveness of using TMD in terms of global structural responses and local energy responses based on 100 simulated earthquake ground motions was studied. Seismic fragility analyses were conducted, and conclusions were drawn based on the simulated results. The results showed that the use of TMD enhances the energy dissipation of the structure over a broad spectrum of earthquake ground motions normalized at PGA of 1.0g by dissipating larger amount of damping energy and lesser amount of plastic energy, which correlates directly to lesser damage in the structure.

While TMD is ineffective in protecting structures against collapse, it has the ability to enhance the fragility of the structure at low to moderate seismic levels. However, there seems to be significant conservatism on the limits of each performance level set forth in FEMA 440 for moment-resisting steel frames. For example, when the immediate occupancy (IO) performance level is reached, the structure remains elastic and it can still withstand larger magnitude earthquakes before yielding begins. In addition, when the collapse prevention (CP) performance level is reached, only moderate strain was observed and the structure still has the capability to

deform further without collapse. Therefore, further research is necessary in standardizing the drift ratio limits of the performance levels.

## REFERENCES

- Abe M. and Fujino Y. (1994). "Dynamic characterization of multiple tuned mass dampers and some design formulas." *Earthquake Engineering and Structural Dynamics*, 23(8), 813-835.
- Bannon H. and Veneziano D. (1982). "Seismic safety of reinforced concrete members and structures." *Earthquake Engineering and Structural Dynamics*, 10(2), 179-193.
- Benavent-Climent A. (2007). "An energy-based damage model for seismic response of steel structures." *Earthquake Engineering and Structural Dynamics*, 36(8), 1049-1064.
- Bojorquez E., Ruiz S.E., and Teran-Gilmore A. (2008). "Reliability-based evaluation of steel structures using energy concepts." *Engineering Structures*, 30(6), 1745-1759.
- Chen G. and Wu J. (2001). "Optimal placement of multiple tuned mass dampers for seismic structures." *Journal of Structural Engineering ASCE*, 127(9), 1054-1062.
- Clough R.W. and Penzien J. (1975). *Dynamics of Structures*, McGraw-Hill, Inc., New York.
- Cosenza E., Manfredi G., and Ramasco R. (1993). "The use of damage functionals in earthquake engineering: a comparison between different methods", *Earthquake Engineering and Structural Dynamics*, 22(10), 855-868.
- Erduran E. and Yakut A. (2007). "Vulnerability assessment of reinforced concrete moment resisting frame buildings." *Journal of Structural Engineering ASCE*, 133(4), 576-586.
- Federal Emergency Management Agency (2005). *Improvement of Nonlinear Static Seismic Analysis Procedures*, FEMA 440.

- Guo Y. and Chen W.Q. (2007). "Dynamic analysis of space structures with multiple tuned mass dampers." *Engineering Structures*, 29(12), 3390-3403.
- Hoang N., Fujino Y., and Warnitchai P. (2008). "Optimal tuned mass damper for seismic applications and practical design formulas." *Engineering Structures*, 30(3), 707-715.
- Hong H.P. and Hong P. (2007). "Assessment of ductility demand and reliability of bilinear single-degree-of-freedom systems under earthquake loading." *Canadian Journal of Civil Engineering*, 34(12), 1606-1615.
- Jarenprasert S., Bazan E., and Bielak J. (2006). "Inelastic spectrum-based approach for seismic design spectra." *Journal of Structural Engineering ASCE*, 132(8), 1284-1292.
- Johnson J.G., Reaveley L.D., and Pantelides, C.P. (2003). "A rooftop tuned mass damper frame." *Earthquake Engineering and Structural Dynamics*, 32(6), 965-984.
- Kafali C. and Grigoriu M. (2007). "Seismic fragility analysis: application to simple linear and nonlinear systems." *Earthquake Engineering and Structural Dynamics*, 36(13), 1885-1900.
- Li C. and Liu Y. (2002). "Active multiple tuned mass dampers for structures under the ground acceleration," *Earthquake Engineering and Structural Dynamics*, 31(5), 1041-1052.
- Li C. and Zhu B. (2007). "Investigation of response of systems with active multiple tuned mass dampers." *Journal of Structural Control and Health Monitoring*, 14(8), 1138-1154.
- Luft R.W. (1979). "Optimal tuned mass dampers for buildings." *ASCE Structural Engineering Division*, 105(12), 2766-2772.
- McCabe S.L. and Hall W.J. (1989). "Assessment of seismic structural damage." *Journal of Structural Engineering ASCE*, 115(9), 2166-2183.
- McNamara R.J. (1977). "Tuned mass dampers for buildings." *ASCE Structural Engineering Division*, 103(9), 1785-1798.

- Nagarajaiah S. and Sonmez E. (2007). "Structures with semi-active variable stiffness single/multiple tuned mass dampers." *Journal of Structural Engineering ASCE*, 133(1), 67-77.
- Nielson B.G. and DesRoches R. (2007). "Seismic fragility methodology for highway bridges using a component level approach." *Earthquake Engineering and Structural Dynamics*, 36(6), 823-839.
- Padgett J.E. and DesRoches R. (2008). "Methodology for the development of analytical fragility curves for retrofitted bridges." *Earthquake Engineering and Structural Dynamics*, 37(8), 1157-1174.
- Park Y.J. and Ang A.H.S. (1985). "Mechanistic seismic damage model for reinforced concrete." *Journal of Structural Engineering ASCE*, Vol. 111(4), 722-739.
- Qin L., Zhou X.Y., and Yan W.M. (2007). "Velocity adjustable TMD and numerical simulation of seismic performance." *Earthquake Engineering and Engineering Vibration*, 6(2), 147-158.
- Simulescu I., Mochio T., and Shinozuka M. (1989). "Equivalent Linearization Method in Nonlinear FEM." *Journal of Engineering Mechanics ASCE*, 115(3), 475-492.
- Uang C.M. and Bertero V.V. (1990). "Evaluation of seismic energy in structures," *Earthquake Engineering and Structural Dynamics*, 19(1), 77-90.
- Ueng J.M., Lin C.C., and Wang J.F. (2008). "Practical design issues of tuned mass dampers for torsionally coupled buildings under earthquake loadings." *The Structural Design of Tall and Special Buildings*, 17(1) 133-165.
- Wang J.F., Lin C.C., and Yen S.M. (2007). "A story damage index of seismically-excited buildings based on modal frequency and mode shape." *Engineering Structures*, 29(9), 2143-2157.

- Wong K.K.F. and Johnson J. (2009). "Seismic energy dissipation of inelastic structures with multiple tuned mass dampers." *Journal of Engineering Mechanics ASCE*, in press.
- Wong K.K.F. and Yang R. (1999). "Inelastic dynamic response of structures using force analogy method," *Journal of Engineering Mechanics ASCE*, 125(10), 1190-1199.
- Xu K. and Igusa T. (1992). "Dynamic characteristics of multiple tuned mass substructures with closely spaced frequencies." *Earthquake Engineering and Structural Dynamics*, 21(12), 1050-1070.
- Yakut A. and Yilmaz H. (2008). "Correlation of deformation demands with ground motion intensity." *Journal of Structural Engineering ASCE*, 134(12), 1818-1828.
- Yeh C.H. and Wen Y.K. (1990). "Modeling of Nonstationary Ground Motion and Analysis of Inelastic Structural Response." *Structural Safety*, 8(1-4), 281-298.
- Zareian F. and Krawinkler H. (2007). "Assessment of probability of collapse and design for collapse safety." *Earthquake Engineering and Structural Dynamics*, 36(13), 1901-1914.

## List of Tables

TABLE 1. Period of Vibration of the Elastic Structure

TABLE 2. Limits of Each Performance Levels

## List of Figures

Figure 1. Elastic and Inelastic Displacements

Figure 2. Six-story moment-resisting steel frame model.

Figure 3. Comparison of time history responses of the frame with and without TMD installed for a single simulated earthquake record at PGA of 1.0g.

Figure 4. Comparison of average maximum kinematic responses of the frame with and without TMD installed due to 100 simulated earthquake records at PGA of 1.0g.

Figure 5. Comparison of average maximum energy responses of the frame with and without TMD installed due to 100 simulated earthquake records at PGA of 1.0g.

Figure 6. Comparison of fragilities of the frame with and without TMD installed at different performance levels.

Figure 7. Correlation of performance level with damage for structure without TMD installed.

Figure 8. Correlation of performance level with damage for structure with TMD of 10% mass.

Figure 9. Correlation of performance level with damage for structure with TMD of 20% mass.

Figure 10 Comparison of local PE Ratios among plastic hinges for structure with and without TMD installed at 50% chance of exceedance of life safety performance level.

Figure 11 Comparison of local PE Ratios among plastic hinges for structure with and without TMD installed at 50% chance of exceedance of collapse prevention performance level.

**TABLE 1. Period of Vibration of the Elastic Structure**

Mode	Period (s)
1	1.22
2	0.44
3	0.25
4	0.18
5	0.14
6	0.11

**TABLE 2. Limits of Each Performance Levels**

Level	Drift Ratio Limit	PE Ratio Limit	Equivalent Monotonic Strain Ductility
IO	0.005	0	1.0
LS	0.01	0.002	2.6
CP	0.02	0.02	17.0

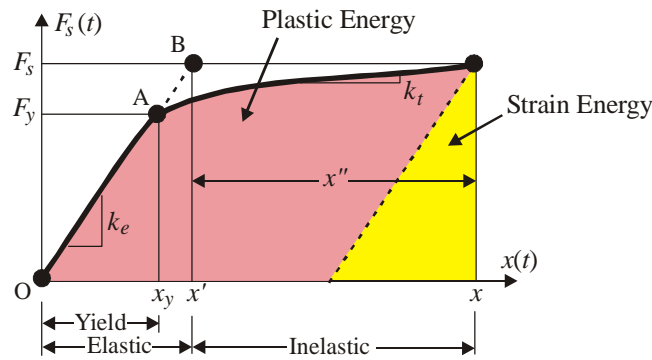


Figure 1. Elastic and inelastic displacements (to be changed).

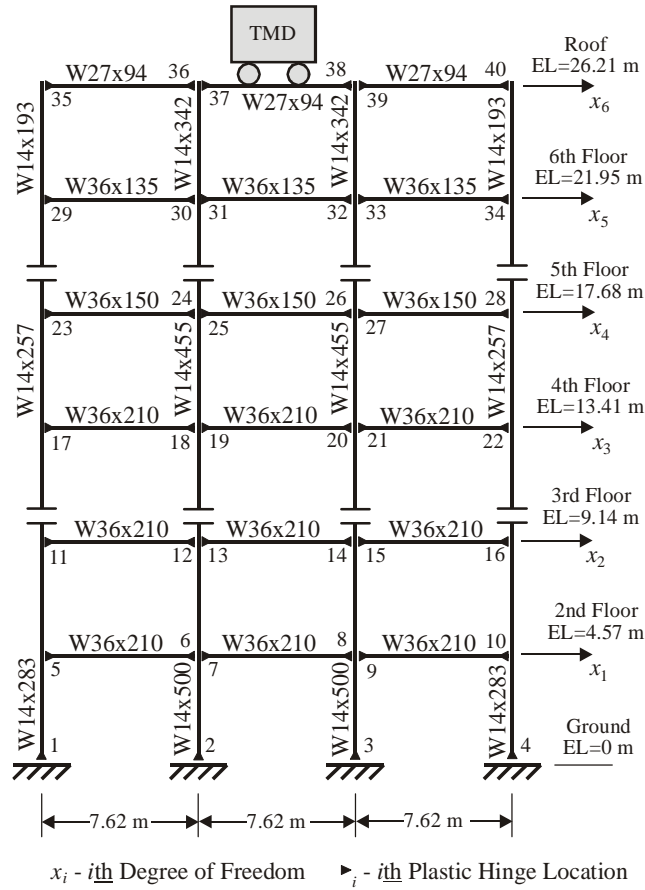


Figure 2. Six-story moment-resisting steel frame model.

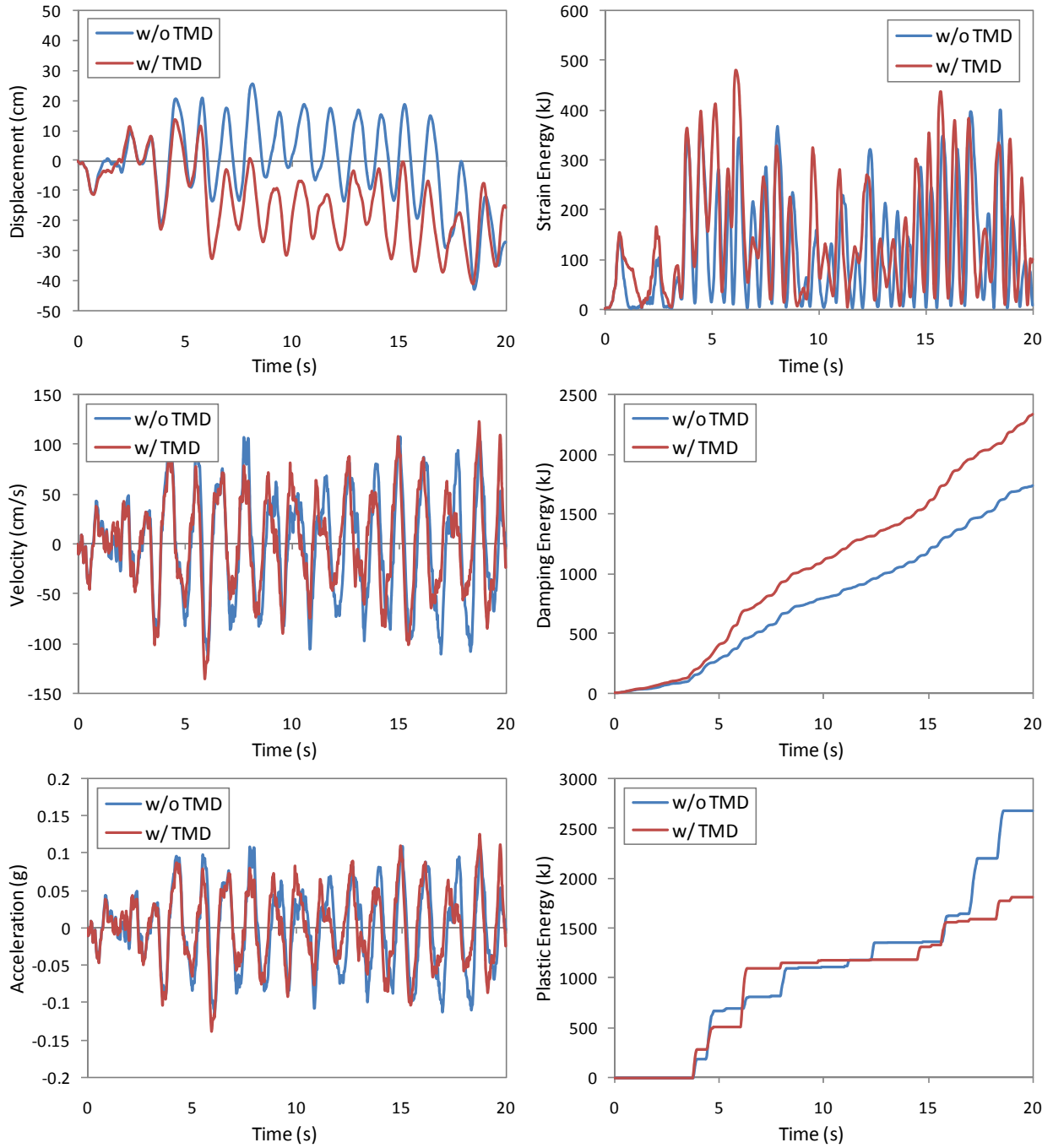


Figure 3. Comparison of time history responses of the frame with and without TMD installed for a single simulated earthquake record at PGA of 1.0g.

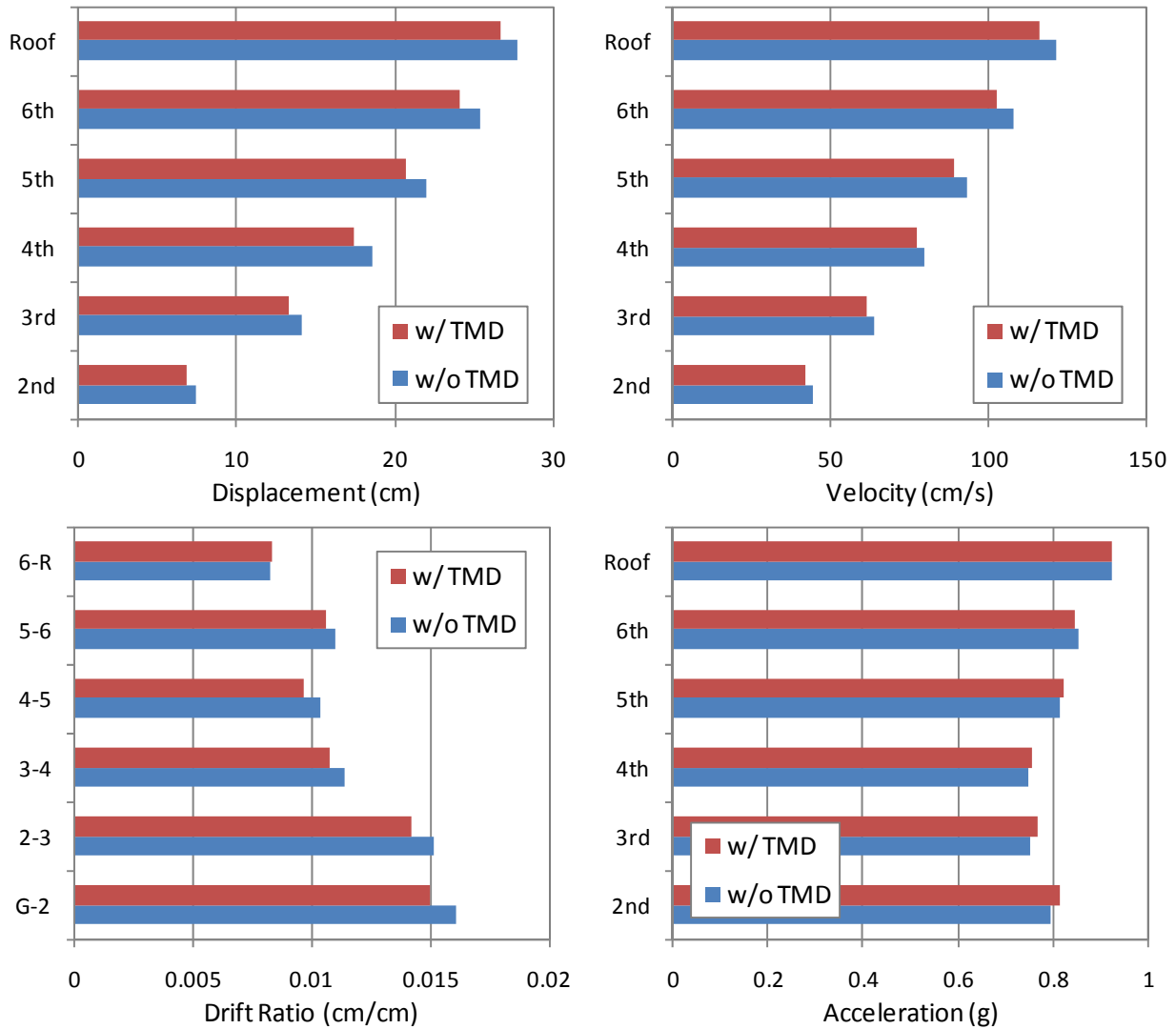


Figure 4. Comparison of average maximum kinematic responses of the frame with and without TMD installed due to 100 simulated earthquake records at PGA of 1.0g.

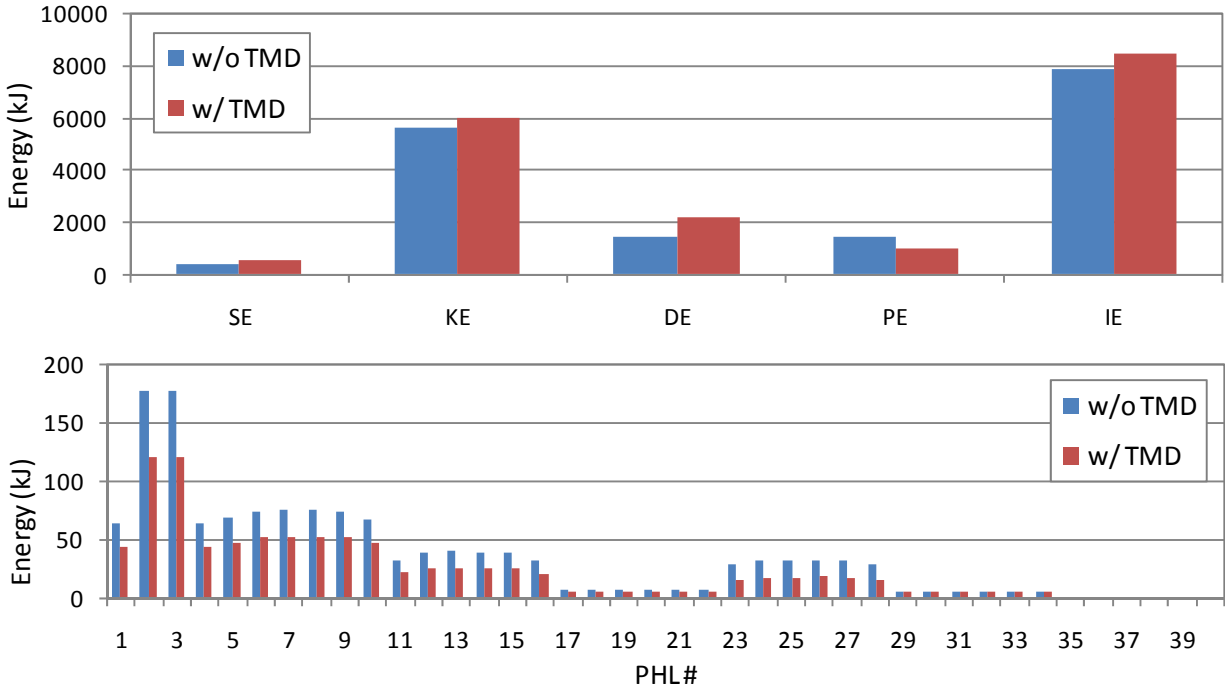


Figure 5. Comparison of average maximum energy responses of the frame with and without TMD installed due to 100 simulated earthquake records at PGA of 1.0g.

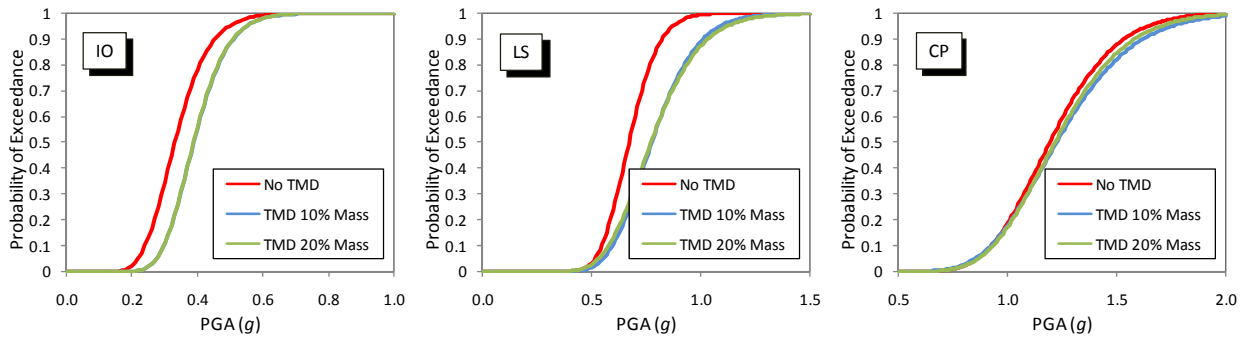


Figure 6. Comparison of fragilities of the frame with and without TMD installed at different performance levels.

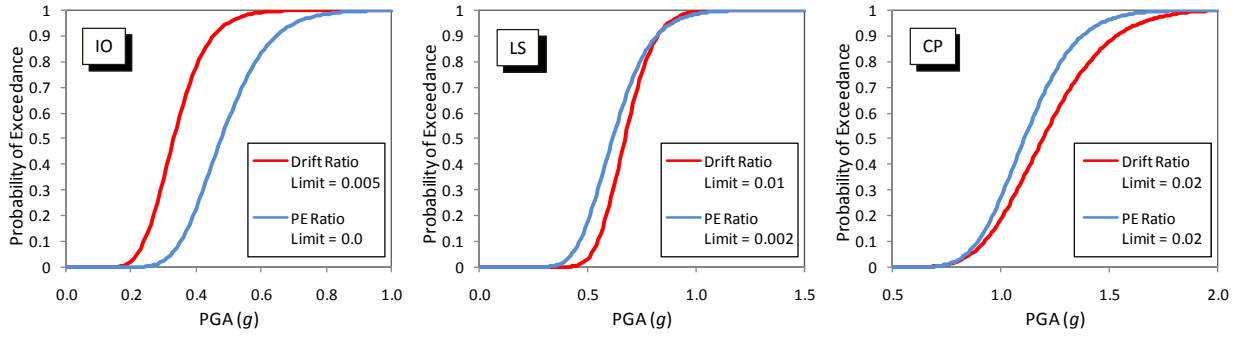


Figure 7. Correlation of performance level with damage for structure without TMD installed.

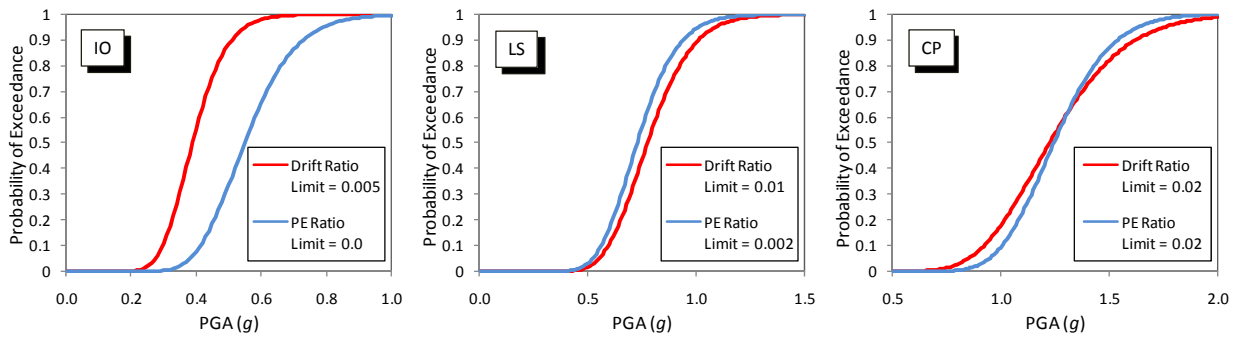


Figure 8. Correlation of performance level with damage for structure with TMD of 10% mass.

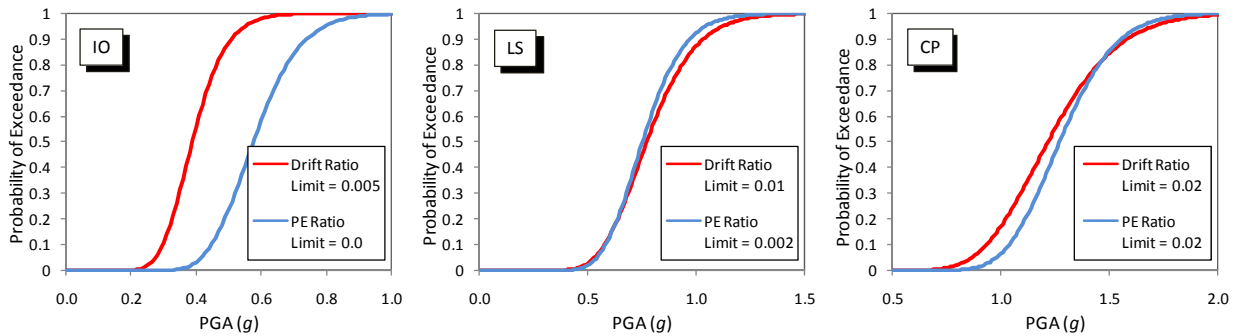


Figure 9. Correlation of performance level with damage for structure with TMD of 20% mass.

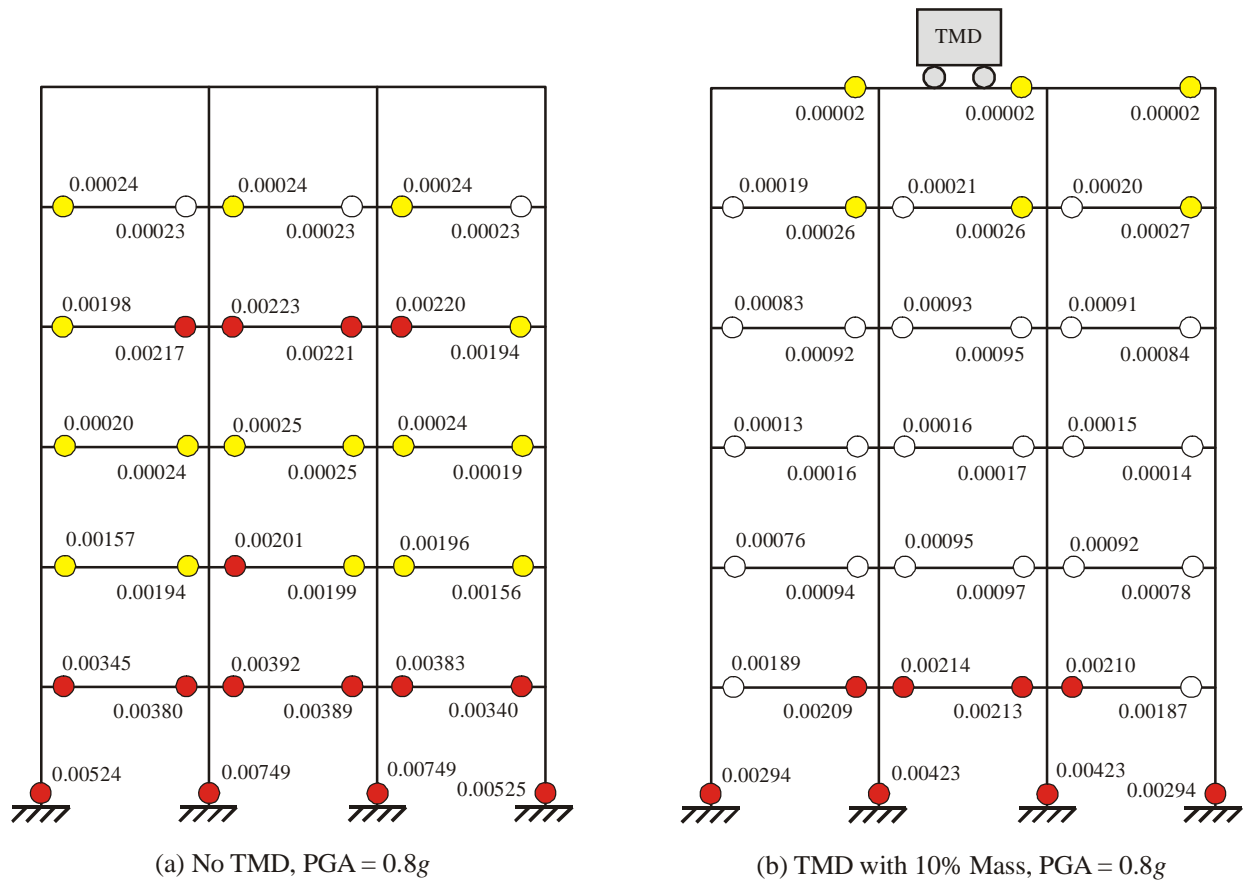


Figure 10 Comparison of local *PE* Ratios among plastic hinges for structure with and without TMD installed at 50% chance of exceedance of life safety (LS) performance level.

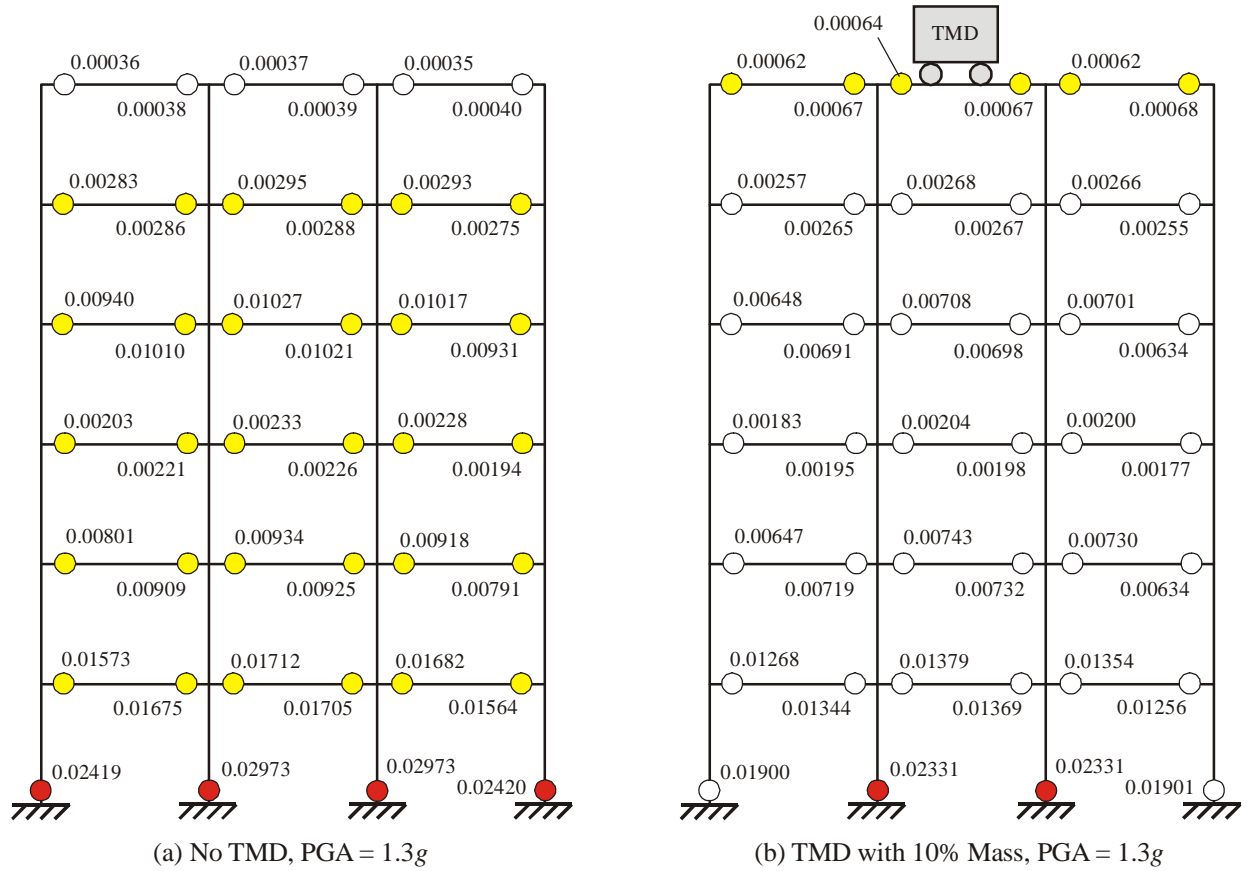


Figure 11 Comparison of local *PE* Ratios among plastic hinges for structure with and without TMD installed at 50% chance of exceedance of collapse prevention (CP) performance level.